frontiers | Frontiers in Nuclear Engineering

TYPE Original Research
PUBLISHED 27 September 2023
DOI 10.3389/fnuen.2023.1236544

OPEN ACCESS

EDITED BY
Taishi Kobayashi,
Kyoto University, Japan

REVIEWED BY
Jun-Yeop Lee,
Pusan National University, Republic of Korea
Arnault Lassin,
Bureau de Recherches Géologiques et Minières, France

*CORRESPONDENCE
Daniela Freyer,
daniela.freyer@chemie.tu-freiberg.de

RECEIVED 07 June 2023
ACCEPTED 23 August 2023
PUBLISHED 27 September 2023

CITATION
Freyer D, Pannach M and Voigt W (2023), Solid–liquid equilibria of Sorel phases and $Mg(OH)_2$ in the system Na-Mg-Cl-OH-H_2O. Part II: Pitzer modeling. *Front. Nucl. Eng.* 2:1236544. doi: 10.3389/fnuen.2023.1236544

Solid–liquid equilibria of Sorel phases and $Mg(OH)_2$ in the system Na-Mg-Cl-OH-H_2O. Part II: Pitzer modeling

Daniela Freyer*, Melanie Pannach and Wolfgang Voigt

TU Bergakademie Freiberg, Institut für Anorganische Chemie, Freiberg, Germany

For geochemical calculations of solubility equilibria between Sorel phases, $Mg(OH)_2$, and oceanic salt solutions, the polythermal THEREDA dataset (based on the HMW model at 25°C) was extended. With both models, H^+ solution concentrations in equilibrium with $Mg(OH)_2$(s) and the 3-1-8 Sorel phase at 25°C can be calculated in good agreement. In contrast, calculated OH^- solution concentrations do not agree. Using the solubility constants (lg Ks) determined up to 60°C in Part I of this work, together with available solubility isotherms up to 120°C, temperature functions for the 3-1-8 phase (25°C–100°C), 2-1-4 phase (60°C–120°C), and 9-1-4 phase (100°C–120°C) were derived. In order to accurately model the OH^- solution concentrations, it was necessary to implement the solution species $Mg_3(OH)_4^{2+}$ ($\Delta_R G_m^\circ$ temperature function) in addition to the $MgOH^+$ already contained in the previous model. Finally, fitting Pitzer mixing coefficients for both species now allow the calculation of the solubility equilibria of $Mg(OH)_2$(s) and the Sorel phases in agreement with the experimental data in the Mg-Cl-OH-H_2O and Na-Mg-Cl-OH-H_2O systems.

KEYWORDS

Pitzer modeling, system Na-Mg-Cl-OH-H_2O, system Mg-Cl-OH-H_2O, magnesium chloride hydroxides, Sorel phases, $Mg(OH)_2$

1 Introduction

Geochemical modeling is an integral tool in the safety assessment of radioactive waste repositories in deep geological formations. The long-term stability of geotechnical barriers and backfill materials must be confirmed under relevant geochemical conditions, such as a saline host rock in the presence of a complex salt solution. Sorel phases are the binder phases of MgO-based building material used for constructing geotechnical barriers (plugs and sealing systems) in the host of rock salt. With the experimentally determined solid–liquid equilibria of Sorel phases and $Mg(OH)_2$(s) in Part I of this work (Pannach et al., 2023), including the data of Altmaier et al. (2003) and Pannach et al. (2017), the long-term stability of magnesia building material (Sorel phases) in contact with solutions in a saline environment (NaCl saturated with already-minor concentrations of $MgCl_2$) has been proven. These data, together with those of $Mg(OH)_2$(s), allow an extension of the geochemical dataset of Pitzer's ion interaction model (Pitzer, 1991) to calculate the solubility equilibria of Sorel phases and $Mg(OH)_2$(s) in solutions of the oceanic salt system. They also allow the calculation of the pH_m values (-lg m (H^+) = pH_m) that evolve in the presence of Sorel phases or $Mg(OH)_2$. The weakly alkaline milieu generated offers favorable geochemical conditions (e.g., by buffering the pH and limiting

carbonate concentration) to minimize radionuclide transport processes via potential salt solutions.

The first Pitzer dataset was developed by Harvie et al. (1984) (HMW model) for modeling mineral solubilities in the complex system of Na-K-Mg-Ca-H-Cl-SO_4-OH-HCO_3-CO_3-CO_2-H_2O at 25°C. The model contains ion interaction coefficients and standard Gibbs energies for aqueous solution species such as $MgOH^+$ and for solid phases like $Mg(OH)_2$ (brucite) and the 3-1-8 Sorel phase ($3Mg(OH)_2{\cdot}MgCl_2{\cdot}8H_2O$ = 2 $Mg_2Cl(OH)_3{\cdot}4H_2O$, korshunovskite).

The HMW model valid for 25°C was used in 2006 as the basis for developing a polythermal THEREDA database of the system Na-K-Mg-Ca-H-Cl-SO_4-CO_3-OH-H_2O for a temperature range of 0°C–100°C (for certain subsystems, the range is extended to 200°C or 250°C). The main objective of THEREDA was to provide a comprehensive and internally consistent thermodynamic reference database for the geochemical modeling of near- and far-field processes in radioactive waste repositories in rock formations currently under discussion in Germany. For the host rock salt, THEREDA is the only database in the world that provides a polythermal model that covers the entire system of oceanic salts, including acids and bases (Voigt et al., 2007; www.thereda.de).

2 Previous data and model situation

The THEREDA model contains some improvements for the oceanic system to the underlying HMW model at 25°C. Examples are: the correct chemical formula of kainite is used ($4KCl{\cdot}4MgSO_4{\cdot}11H_2O$ instead of $KCl{\cdot}MgSO_4{\cdot}3H_2O$); the missing mineral goergeyite ($K_2SO_4{\cdot}5CaSO_4{\cdot}H_2O$) is included, which has a crystallization field at 298 K; the solubility of KCl is described more correctly; the water activity of gypsum/anhydrite transition at NaCl saturation is shifted to the more acceptable value of 0.84–0.85 (instead of 0.775 in the HMW model); two additional aqueous solution species ($KMgSO_4^+$ and $KCaSO_4^+$) have been implemented, which was necessary in order to describe solubilities at enhanced temperatures.

As the solubility of $Mg(OH)_2$(s) in water is $m_{Mg(OH)2} < 2{\cdot}10^{-5}$, experimental data such as activity and osmotic coefficients are not available to determine binary Pitzer coefficients. Since sufficient data from ternary systems containing magnesium and hydroxide were not available until 2017, no parameters could be derived from these systems either. The temperature-dependent parameters given in THEREDA had been derived from adjustments to the solubility data of the binary system $Mg(OH)_2$-H_2O. As per Harvie et al. (1984) for 25 °C, the solubility constant of $Mg(OH)_2$(s) was adapted from the data of McGee and Hostetler (1977) (values up to 90°C) fitting the temperature function up to 250°C to the solubility data of the system $Mg(OH)_2$-H_2O (Travers, 1929; Lambert and Clever, 1992). Analogous to HMW, all binary interactions Mg^{2+}-OH^- were assigned to the complex species $MgOH^+$. Its temperature function was adapted according to the stability constants published by Palmer and Wesolowski (1997). Due to the lack of data before 2017 for the system $Mg(OH)_2$-$MgCl_2$-H_2O at higher temperatures, parameters and the solubility constant for the Sorel phase 3-1-8 could only be given for 25°C and were taken unchanged from Harvie et al. (1984).

In the comparing HMW and THEREDA, the deviation in the description of the solubility of $Mg(OH)_2$ and the 3-1-8 phase at 25°C in the ternary Mg-Cl-OH-H_2O system (Figure 1A) is mainly due to the deviating stability constant of the complex species $MgOH^+$, which originates from the re-determination of Palmer and Wesolowski (1997). Figure 1A shows the newer solubility data from Pannach et al. (2017); as discussed there, the experimental data determined by Robinson and Waggaman (1909) are generally too low. The calculated isotherms with both HMW and THEREDA for the ternary system Mg-Cl-OH-H_2O describe quite well the invariant point of $Mg(OH)_2$ and the 3-1-8 phase at 1.75 m_{MgCl2} but not the experimentally determined OH^- solution concentrations (Pannach et al., 2017) over the entire $MgCl_2$ concentration range. The model values in the presence of $Mg(OH)_2$(s) and the 3-1-8 phase up to 3.5 m_{MgCl2} are too low, and above are too high. This is because Harvie et al. (1984) is fitted to the solubility data of D'Ans et al. (1955) (open symbols in Figure 1). However, these data do not belong to the ternary system but to the NaCl-containing Na-Mg-Cl-OH-H_2O due to the use of NaOH solution to precipitate the solids from the different $MgCl_2$ solutions.

In NaCl-saturated $MgCl_2$ solutions, the OH^- concentrations (given as $Mg(OH)_2$ molality in the diagrams, representative of half of the OH^- solution concentration) are generally calculated too high, as can be seen in Figure 1B, in comparison with the experimental data from Part I of this work (Pannach et al., 2023) and the data of D'Ans et al. (1955) at unknown NaCl concentrations.

Contrary to OH^-, the H^+ concentrations (as -lg m (H^+) = pH_m) in equilibrium with $Mg(OH)_2$(s) and 3-1-8 phase calculated by both models agree with the experimental data (Figure 2). The agreement between modeled and experimental results is clear in both logarithmic and non-logarithmic plots (the latter is not illustrated).

In summary, neither the HMW nor the THEREDA model sufficiently describes the OH^- concentrations in equilibrium with $Mg(OH)_2$(s) and the Sorel phase. Hence, with the new experimental data, with OH^- equilibrium concentrations in the Mg-Cl-OH-H_2O system up to 120°C (Pannach et al., 2017), in the Na-Mg-Cl-OH-H_2O system up to 40°C, and the solubility constants of Sorel phases at 25°C, 40°C, and 60°C (Part I of this paper—Pannach et al., 2023), the model was adjusted and expanded; this included the Sorel phases 3-1-8, 9-1-4, and 2-1-4, and the metastable 5-1-8 phase.

3 Procedure for model adjustment

For fitting and extending the model, the solubility constants of the Sorel phases (Part I of this work) were first implemented in a test dataset. These K_S values were further constrained within their given uncertainty range by fitting them to the experimentally available invariant points (IP) at the corresponding $MgCl_2$ concentration (or the $MgCl_2$ concentration range in which they are expected) in the Mg-Cl-OH-H_2O (Pannach et al., 2017) and Na-Mg-Cl-OH-H_2O systems (Part I of this work). At first, the lgK_S of the 3-1-8 phase was constrained by the IP with $Mg(OH)_2$(s), which is possible because the lgK_S of $Mg(OH)_2$(s) is fixed in the THEREDA dataset. Using the lgK_S of the 3-1-8 phase thus fixed, lgK_S of the 2-1-4 was then refined using their common IPs (3-1-8 + 2-1-4). At higher temperatures of 100°C and 120°C, where $Mg(OH)_2$(s) borders the 9-1-4 phase, their IPs were used to determine the lgK_S values of the 9-1-4 phase. At

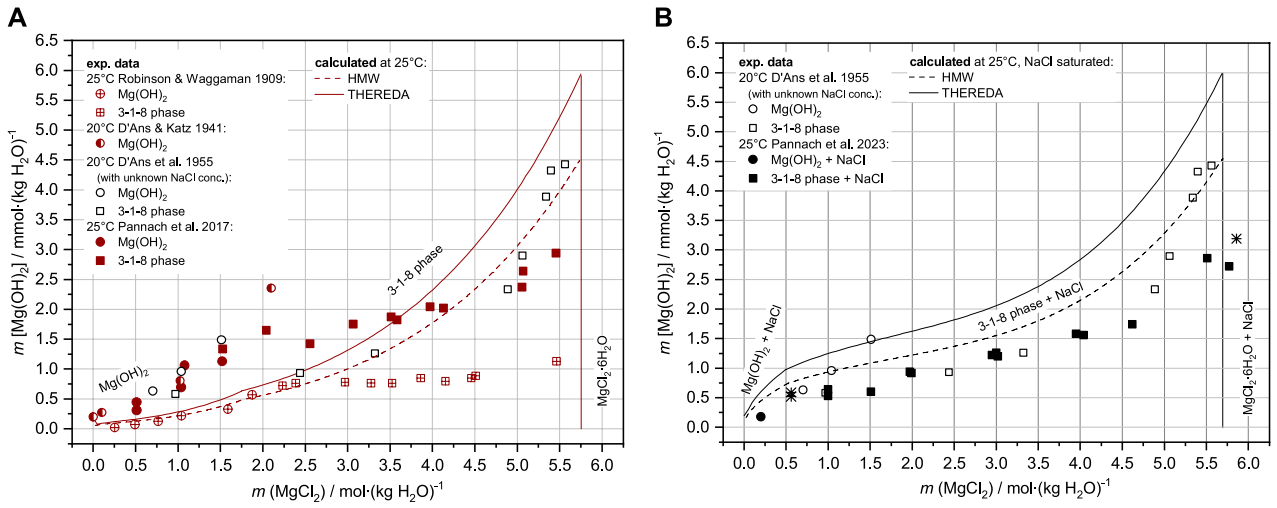

FIGURE 1
Solubility data for the Mg-Cl-OH-H_2O system **(A)** and the Na-Mg-Cl-OH-H_2O system **(B)** at 25 °C and the data from D'Ans et al. at 20 °C compared to the HMW and THEREDA models.

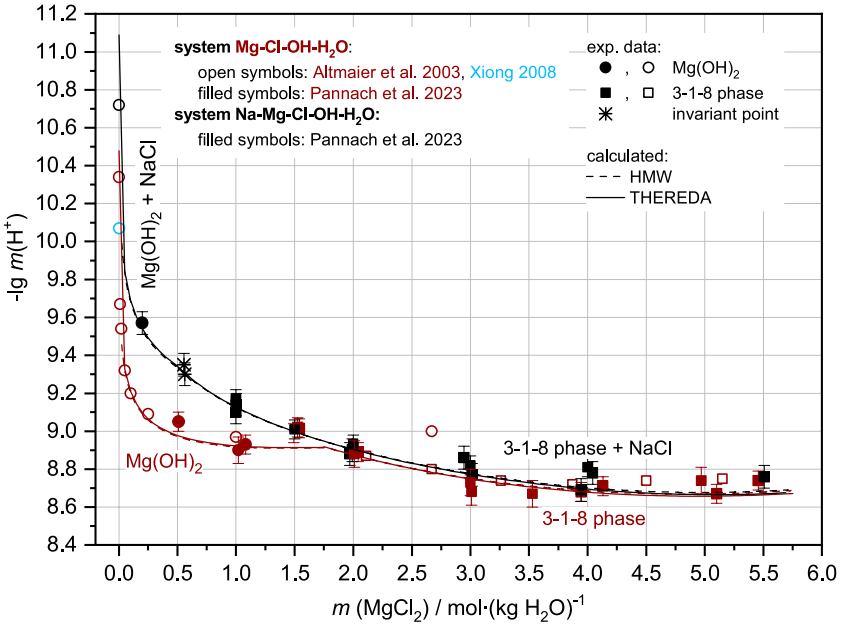

FIGURE 2
Comparison between H^+ equilibrium concentrations as -lg m (H^+) = pH_m from experimental data and HMW and THEREDA models for the Mg-Cl-OH-H_2O (brown symbols and line) and Na-Mg-Cl-OH-H_2O systems at NaCl saturation (black symbols and line) at 25°C.

these two temperatures, IPs of the 9-1-4 and 2-1-4 phases were then used to determine the lgK_S of the 2-1-4 phase at 100°C and 120°C. More precise K_S and $\Delta_R G_m$ values were thus obtained with significantly smaller corresponding errors. A temperature function was then derived from the single $\Delta_R G_m^\circ$ values of each Sorel phase and finally implemented in the THEREDA dataset (Section 4.1). The second step (Section 4.2) was to fit the Pitzer parameters in the presence of the fixed solubility constants, where it became apparent that an extension of the OH^- speciation model was also necessary (Section 4.2.2). Only then was it possible to successfully fit Pitzer parameters to reproduce the OH^- solution concentrations of both systems (Section 4.2.3).

All calculations were performed using the ChemSage (Eriksson and Hack, 1990) or ChemApp (Eriksson et al., 1997) codes. For adjustments, a specially written C-program was used, implemented in ChemApp, to calculate the smallest error sum of squares between the experimental and calculated values for up to three parameters to be changed, within the specified limits for all possible combinations.

TABLE 1 Overview of solid phases, solution species, and ion interactions already provided in THEREDA for the title system by molal standard Gibbs energies of reaction ($\Delta_R G_m^\circ$) and Pitzer coefficients. Note that, for all Primary Master species in THEREDA, $\Delta_R H^\circ_{i,T=T0}$, $\Delta_R S^\circ_{i,T=T0}$ = 0, and thus $\Delta_R G^\circ_{i,T=T0}$ = 0. Primary Master species of the title system are Na^+, Mg^{2+}, Cl^-, H^+, and H_2O (all further species and solids are formed from them by corresponding formation reactions).

$\Delta_R G_m^\circ$ for solids				
NaCl	Temperature function, 0°C–200°C			
$MgCl_2.6H_2O$	Temperature function, 0°C–120°C			
$Mg(OH)_2$	Temperature function, 0°C–250°C			
$Mg_2(OH)_3Cl{\cdot}4H_2O$	*At 25°C*			
$\Delta_R G_m^\circ$ for solution species				
OH^-	Temperature function, 0°C–250°C			
$MgOH^+$	Temperature function, 0°C–250°C			
Ion interaction coefficients				
i	**j**	**$\beta^{(0)}_{ij}$**	**$\beta^{(1)}_{ij}$**	**C^φ_{ij}**
H^+	Cl^-	Temperature functions, 0°C–120°C		
Na^+	Cl^-	Temperature functions, 0°C–200°C		
Mg^{2+}	Cl^-	Temperature functions, 0°C–120°C		
$MgOH^+$	*Cl^-*	*25 °C*	*25 °C*	-
Na^+	OH^-	Temperature functions, 0°C–120°C		
i	**j**	**k**	**θ_{ij}**	**ψ_{ijk}**
Na^+	Mg^{2+}	Cl^-	Temperature functions, 0°C–120°C	
H^+	Na^+	Cl^-	Temperature functions, 0°C–120°C	
H^+	Mg^{2+}	Cl^-	Temperature functions, 0°C–120°C	
$MgOH^+$	*Na^+*	*Cl^-*	-	-
$MgOH^+$	*Mg^{2+}*	*Cl^-*	-	*25°C*
OH^-	Cl^-	Na^+	Temperature functions, 0°C–120°C	

This was applied to determine the final Pitzer parameters, with subsequent fine-tuning performed on the optical trend of each isotherm.

4 THEREDA model adaption on Sorel phases

For the title system, the THEREDA model already contains molal standard Gibbs energies $\Delta_R G_m^\circ$, which correspond to the solubility constants K_s, (Eq. 1), as well as the Pitzer coefficients as summarized in Table 1.

$$\Delta_R G_m^\circ = -R \cdot T \cdot \ln K_S \quad \text{resp.} \quad \Delta_R G_m^\circ = -2.303 \cdot R \cdot T \cdot \lg K_S. \quad (1)$$

Where the data in Table 1 are written in non-italics, no changes were made for the extension of THEREDA by the Sorel phases, as subsystems such as NaCl-H_2O, $MgCl_2$-H_2O, $Mg(OH)_2$-H_2O, NaOH-H_2O, and NaCl-$MgCl_2$-H_2O were already described well by the model.

4.1 Solubility constants and T-functions for Sorel phases

Solubility constants for the Sorel phases at different temperatures are available from Part I of this work (Pannach et al., 2023) and are shown in Table 2. The values in bold are used for model parameterization.

4.1.1 Sorel phase 3-1-8

The standard Gibbs energy proposed by the HMW model (Harvie et al., 1984) and the corresponding solubility constant for the reaction:

$$2\,Mg^{2+} + Cl^- + 7\,H_2O \rightleftharpoons Mg_2Cl(OH)_3 \cdot 4\,H_2O_{(s)} + 3\,H^+ \quad (2)$$

$$lgK^\circ_{S,3-1-8} = -26.03$$

is already contained in the THEREDA model and is within the error range, with the overall mean value lg $K_{S,3\text{-}1\text{-}8,25°C}$ = −26.1 ± 0.2 at 25°C given in Table 2. From this value, $\Delta_R G_m^\circ$ = 149.0 ± 1.1 kJ mol^{-1} is calculated. To fix the value within the error range, the invariant point (IP) of $Mg(OH)_2$(s) and 3-1-8 phase in the Na-Mg-Cl-OH-H_2O system (at NaCl saturation) experimentally determined in Part I was used (none is available from the ternary Mg-Cl-OH-H_2O system). To reproduce this IP at 0.56 ± 0.1 m_{MgCl2} by the model, $\Delta_R G_{m,25°C}^\circ$ narrows to 148.7 ± 0.1 kJ mol^{-1}, which corresponds to lg *Ks* = −26.046 ± 0.011 (Figure 3).

No experimental IP of the $Mg(OH)_2$(s) and 3-1-8 phase is available to refine the $\Delta_R G_{m,40°C}^\circ$ (148.7 ± 1.2 kJ mol^{-1}) calculated from the solubility constant at 40 °C (lg $K_{S,3\text{-}1\text{-}8,40°C}$ = −24.8 ± 0.2). However, according to the solubility data for $Mg(OH)_2$ and the 3-1-8 phase, the IP is expected to be between 1.6 and 2.0–2.5 m_{MgCl2} in the Mg-Cl-OH-H_2O system and between 1.0 and 1.5 m_{MgCl2} in the NaCl-saturated solutions (Na-Mg-Cl-OH-H_2O system) at 40°C. To ensure that the model does not slip below 1.0 m_{MgCl2} at NaCl saturation and remains in the IP range for the Mg-Cl-OH-H_2O system, $\Delta_R G_{m,40°C}^\circ$ cannot exceed 147.7 kJ mol^{-1}, which corresponds to the lower error limit resulting from $K_{S,3\text{-}1\text{-}8,40°C}$ (Figure 3).

At 60°C, only solubility data in the Mg-Cl-OH-H_2O system are available to fix $\Delta_R G_{m,60°C}^\circ$ calculated from the mean value of the solubility constant lg $K_{S,3\text{-}1\text{-}8,60°C}$ = −23.04 ± 0.11 (Table 2) resulting in 147.0 ± 0.7 kJ mol^{-1}. The IP of $Mg(OH)_2$(s) and the 3-1-8 phase is expected between 2.6 and 3.0 m_{MgCl2}, which limits $\Delta_R G_{m,60°C}^\circ$ to 146.3 ± 0.2 kJ mol^{-1}.

At 80 °C, no solubility constant is available, so the IP of $Mg(OH)_2$(s) and the 3-1-8 phase in the Mg-Cl-OH-H_2O system is expected to be between 3.2 and 4.0. In addition, the experimentally determined IP of the 3-1-8 and 2-1-4 phases was found at 5.8 m_{MgCl2}. This concentration should be reproduced by the model with ±0.1 m_{MgCl2} alongside the expected IP range of the $Mg(OH)_2$(s) and 3-1-8 phase, constraining $\Delta_R G_{m,80°C}^\circ$ to 144.5 ± 0.2 kJ mol^{-1} (re-calculating lg $K_{S,3\text{-}1\text{-}8,80°C}$ = −21.369 ± 0.011).

Using all the determined values for $\Delta_R G_{m,3\text{-}1\text{-}8}^\circ$ for the different temperatures (open squares in Figure 3), the THEREDA-conforming temperature function

TABLE 2 Solubility constants (lg K_S) for the Sorel phases 3-1-8, 5-1-8 and 2-1-4 determined in Part I of this work (Pannach et al., 2023) compared to available data from the literature. The values in bold are used for model fitting. No data are available for the 9-1-4 phase.

Sorel phase	T [°C]	System Mg-Cl-OH-H_2O		System Na-Mg-Cl-OH-H_2O		Overall mean value, lg K_S
		lg $K_S \pm \sigma$	Ref	lg $K_S \pm \sigma$	Ref	
3-1-8 phase	**25**	−26.15 ± 0.16	Altmaier et al. (2003)	−26.16 ± 0.13	*Part I of this work*	**−26.1 ± 0.2**
		−26.10 ± 0.13	*Part I of this work*			
	40	−24.72 ± 0.04	*Part I of this work*	−24.88 ± 0.16	*Part I of this work*	**−24.8 ± 0.2**
	60	**−23.04 ± 0.11**	*Part I of this work*	-		
5-1-8 phase	**25**	−43.39 ± 0.25	*Part I of this work*	−43.21 ± 0.33	Xiong et al. (2010)	**−43.3 ± 0.3**
2-1-4 phase	**60**	**−32.95 ± 0.20**	*Part I of this work*	-		

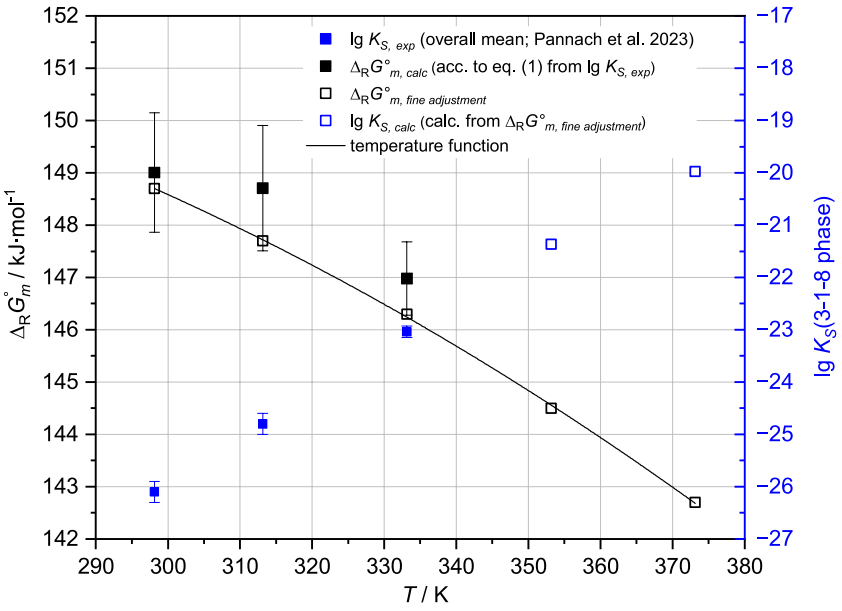

FIGURE 3
$\Delta_R G_m^\circ$ function of the 3-1-8 phase resulting from the single isotherm values of the experimentally determined lg $K_{S,3\text{-}1\text{-}8}$ at 25°C, 40°C, and 60°C, together with available solubility data, the positions of IP's with this phase up to 100°C in the Mg-Cl-OH-H_2O system, and at 25°C and 40°C in the Na-Mg-Cl-OH-H_2O system (Pannach et al., 2017; Pannach et al., 2023).

$$\Delta_R G_m^\circ = A + B \cdot T + C \cdot T \cdot \ln(T) + D \cdot T^2 + E \cdot T^3 + \frac{F}{T} \quad (3)$$

was fitted and extrapolated to 100°C. According to the experimental data at 100°C, the 3-1-8 phase is replaced by the 9-1-4 phase (Pannach et al., 2017). In order to model the metastable range, the $\Delta_R G_m^\circ$ obtained by extrapolation had to be slightly shifted to $\Delta_R G_{m,100°C}^\circ$ = 142.8 kJ mol^{-1}. The finally fitted $\Delta_R G_{m,3\text{-}1\text{-}8}^\circ$ (T) function (Table 3) calculates $\Delta_R G_{m,100°C}^\circ$ = 142.59 kJ mol^{-1} and is shown in Figure 3 together with all single values at the different temperatures.

4.1.2 Sorel phase 2-1-4

The Sorel phase 2-1-4 is stable from 60 °C and was found in the Mg-Cl-OH-H_2O system at higher $MgCl_2$ solution concentrations during the investigations of Pannach et al. (2017). The solubility constant according to the formation reaction in Eq. 4 was determined in Part I of this work at 60 °C (Table 2).

$$3\,Mg^{2+} + 2\,Cl^- + 8\,H_2O \rightleftharpoons Mg_3Cl_2(OH)_4 \cdot 4\,H_2O_{(s)} + 4\,H^+ \quad (4)$$

Analogous to the evaluation of the $\Delta_R G_m^\circ$ function of the 3-1-8 phase, further values of $\Delta_R G_m^\circ$ for the 2-1-4 phase were derived from the available solubility data up to 120°C.

The solubility constant lg $K_{S,2\text{-}1\text{-}4,60°C}$ = −32.95 ± 0.20 (Table 2) corresponds to $\Delta_R G_{m,2\text{-}1\text{-}4,60°C}^\circ$ = 210.2 ± 1.3 kJ mol^{-1}. From the solubility data at 60°C, the IP of the 3-1-8 and 2-1-4 phases is expected to be slightly above 5.4 m_{MgCl2} (between 5.4 and 5.7 m_{MgCl2}). To represent this by the model, the $\Delta_R G_{m,2\text{-}1\text{-}4,60°C}^\circ$ needs to be constrained to 211.2 ± 0.1 kJ mol^{-1}. From the solubility data at 80°C, the experimentally determined IP of the 3-1-8 and 2-1-4 phases in 5.8 m_{MgCl2} is available. For a model reproducing the

TABLE 3 Temperature coefficients for the standard Gibbs energy $\Delta_R G_m^\circ$ for the formation of species or phases from ions and water for the title system Na-Mg-Cl-OH-H_2O and subsystem in THEREDA. The new data from this work are highlighted in bold.

$\Delta_R G_m^\circ(T) = A + B{\cdot}T + C{\cdot}T{\cdot}\ln(T) + D{\cdot}T^2 + E{\cdot}T^3 + F/T$							
Formula	**$T_{min-max}$/K**	**A**	**B**	**C**	**D**	**E**	**F**
H_2O	273.15–393.15	0	0	0	0	0	0
H^+	273.15–393.15	0	0	0	0	0	0
Na^+	273.15–393.15	0	0	0	0	0	0
Mg^{2+}	273.15–393.15	0	0	0	0	0	0
Cl^-	273.15–393.15	0	0	0	0	0	0
OH^-	273.15–523.15	977916.173	−24698.7262	4264.428838	−8.43137921	0.003231957	−34104000
$MgOH^+$	273.15–523.15	444044.0813	−5495.03903	798.7412063	0	−0.00052773	−24391000
$Mg_3(OH)_4^{2+}$	**298.15–393.15**	**380640.7744715**	**−1108.926598837**	**0**	**2.666840823399**	**−0.002366734203628**	**0**
$Mg(OH)_2$(s) (brucite)	273.15–393.15	127348.8077	−99.3761865	0	0	0	0
NaCl	273.15–480.15	−1585611	37614.26246	−6327.712366	11.10781391	−0.003763213	71992993
$MgCl_2{\cdot}6H_2O$ (bischofite)	273.15–389.15	4095895.434	−195408.9322	36798.92745	−109.7047406	0.05399217544	0
3-1-8 phase (korshunovskite)	**298.15–373.15**	**144872.5390947**	**87.22354499983**	**0**	**−0.2494948491172**	**0**	**0**
5-1-8 phase	**298.15**	**247202.4585**	**0**	**0**	**0**	**0**	**0**
2-1-4 phase	**333.15–393.15**	**20577.93725001**	**1205.370**	**0**	**−1.90**	**0**	**0**
9-1-4 phase	**373.15–393.15**	**594712.0**	**−480.0**	**0**	**0**	**0**	**0**

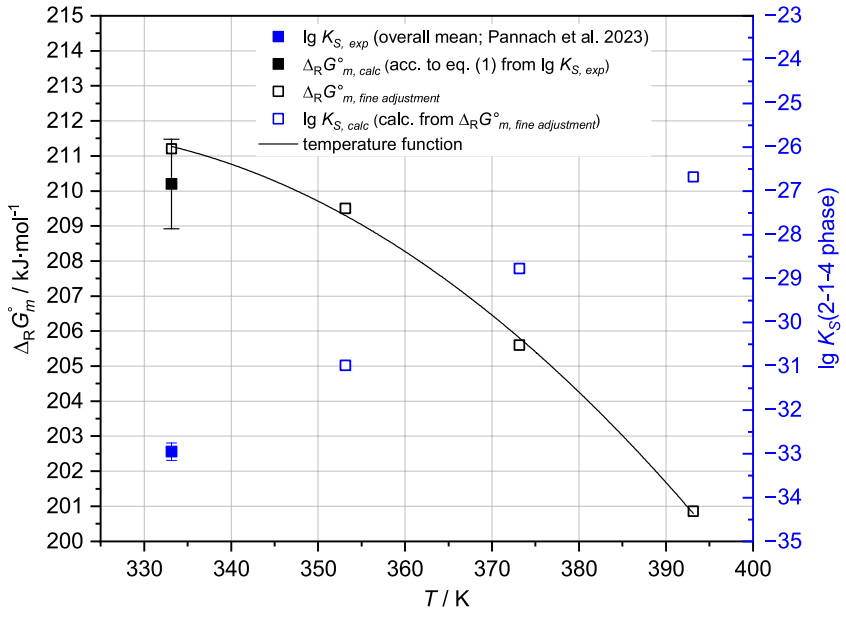

FIGURE 4
$\Delta_R G_m^\circ$ values of the 2-1-4 phase, derived from lg $K_{S,2\text{-}1\text{-}4,60^\circ C}$ at 60°C, and available solubility data at 60°C, 80°C, 100°C, and 120°C in the Mg-Cl-OH-H_2O system (Pannach et al., 2017; Pannach et al., 2023).

IP with ±0.1 m_{MgCl2}, $\Delta_R G_m^\circ{}_{,2\text{-}1\text{-}4,80^\circ C}$ needs to be 209.5 ± 0.1 kJ mol^{-1}.

At 100°C, in addition to the 2-1-4 phase, the 9-1-4 phase occurs as a stable Sorel phase in the Mg-Cl-OH-H_2O system (Pannach et al., 2017). The estimation of the crossing point from the trend of the solubility data of the 9-1-4 and 2-1-4 phases at 100°C suggests the IP at 5.4 ± 0.2 m_{MgCl2}. To represent it by the model, a value of $\Delta_R G_m^\circ{}_{,2\text{-}1\text{-}4,100^\circ C}$ = 205.6 ± 0.1 kJ mol^{-1} needs to be applied.

At 120°C, the IP of the 9-1-4 and 2-1-4 phases was determined at 5.8 m_{MgCl2} (Pannach et al., 2017) and adjusts $\Delta_R G_m^{\circ}{}_{,2\text{-}1\text{-}4,120°C}$ = 200.86 ± 0.1 kJ mol^{-1}.

Using all the values determined at different temperatures, a $\Delta_R G_m^{\circ}{}_{,2\text{-}1\text{-}4}$ temperature function according to Eq. 3 was generated (Figure 4; Table 3).

4.1.3 Sorel phase 9-1-4

The 9-1-4 phase ($9Mg(OH)_2{\cdot}MgCl_2{\cdot}4H_2O = 2\,Mg_5Cl(OH)_9{\cdot}2H_2O$) occurs above 80°C. Solubility data for the 9-1-4 phase are available at 100°C and 120°C, including IPs with $Mg(OH)_2$(s) for both temperatures, as well as with the 2-1-4 phase at 120°C. However, unlike the 3-1-8 or 2-1-4 phases, there are no solubility constants available. For an initial estimation of lg $K_{S,9\text{-}1\text{-}4}$ values, the IPs with $Mg(OH)_2$(s) were used, as the 9-1-4 phase formation according to reaction (5) is in equilibrium with $Mg(OH)_2$(s) at the same $MgCl_2$ concentration (at 100°C: 4.04 m_{MgCl2} and 120°C: 4.00 m_{MgCl2} (Pannach et al., 2017)). The solubility constants were calculated according to Eq. 6 using the activity coefficients γ_i of Mg^{2+} and Cl^- and the activities for water (a_W), and H^+ ($a_{H+} = m_{H+} \cdot \gamma_{H+}$) calculated by THEREDA for these $MgCl_2$ concentrations at 100°C and 120°C. This results in lg $K_{S,9\text{-}1\text{-}4,100°C} = -58.2$ and lg $K_{S,9\text{-}1\text{-}4,120°C} = -53.9$, which correspond to $\Delta_R G_m^{\circ}{}_{,9\text{-}1\text{-}4,100^{\circ}}$ = 415.5 kJ/mol and $\Delta_R G_m^{\circ}{}_{,9\text{-}1\text{-}4,120^{\circ}}$ = 405.9 kJ/mol according to Eq. 1.

$$5\,Mg^{2+} + Cl^- + 11\,H_2O \rightleftharpoons Mg_5Cl(OH)_9 \cdot 2H_2O_{(s)} + 9\,H^+ \quad (5)$$

$$lgK^{\circ}_{S,9-1-4} = lg\left(\frac{m^9_{H^+}}{m^5_{Mg^{2+}} \cdot m_{Cl^-}} \cdot \frac{\gamma^9_{H^+}}{\gamma^5_{Mg^{2+}} \cdot \gamma_{Cl^-}} \cdot \frac{1}{a^{11}_W}\right). \quad (6)$$

Both "initial values" were adjusted to the position of the IPs of $Mg(OH)_2$(s) and the 9-1-4 phase in 4.0 molal $MgCl_2$ solution at 100°C and 120°C respectively, and to the IP of 9-1-4 and 2-1-4 phase at 120°C in 5.8 m_{MgCl2} (Pannach et al., 2017). The final Gibbs energies are $\Delta_R G_m^{\circ}{}_{,9\text{-}1\text{-}4,100°C}$ = 415.60 kJ mol^{-1} and $\Delta_R G_m^{\circ}{}_{,9\text{-}1\text{-}4,120°C}$ = 406.00 kJ mol^{-1}, respectively, and agree well with the previously calculated values. A linear temperature function was generated for the small temperature range of 100°C–120°C (Table 3).

4.1.4 Metastable Sorel phase 5-1-8

The 5-1-8 phase forms from OH^- supersaturated $MgCl_2$ or NaCl-$MgCl_2$ solutions before the stable 3-1-8 phase crystallizes (Pannach et al., 2017; 2023). Within the time window of metastable existence, the lg $K_{S,5\text{-}1\text{-}8}$ according to Eq. 7 could be determined at 25°C from pH_m measurements in the Na-Mg-Cl-OH-H_2O system by Xiong et al. (2010) and in the Mg-Cl-OH-H_2O system in Part I of this work (Pannach et al., 2023). The mean values of both, which agree within the error range (see Table 2), were implemented in the THEREDA model as $\Delta_R G_m^{\circ}{}_{,5\text{-}1\text{-}8,25°C}$ calculated according to Eq. 1; (Table 3).

$$3\,Mg^{2+} + Cl^- + 9\,H_2O \rightleftharpoons Mg_3Cl(OH)_5 \cdot 4\,H_2O_{(s)} + 5\,H^+ \quad (7)$$

4.2 Adaptation of the model to reproduce the experimental OH^- solution concentrations

As described in Chapter 2, the current model dataset (HMW as well as THEREDA) cannot reproduce the experimentally determined OH^- solution concentrations in the presence of $Mg(OH)_2$(s) or the Sorel phases (up to the order of 100% deviation) at 25°C, and also not at higher temperatures after implementation of the $\Delta_R G_m^{\circ}$ temperature functions of the Sorel phases as observed in initial test calculations. All the calculated OH^- solution concentrations were significantly too low.

However, the calculated H^+ equilibrium concentrations are in excellent agreement with the experimental values, which are available up to 60°C for the Mg-Cl-OH-H_2O system and at 25°C and 40°C for the Na-Mg-Cl-OH-H_2O system, as shown in Figures 8, 9 respectively (see Section 5.1).

4.2.1 Attempts to adjust already existing Pitzer coefficients

To improve the model, attempts were made to adjust Pitzer coefficients that affect the OH^- solution concentrations in $MgCl_2$ and NaCl-$MgCl_2$ solutions. According to the HMW model, THEREDA already contains the binary coefficients $\beta^{(0)}$ and $\beta^{(1)}$ between $MgOH^+$ and Cl^-, and the mixing coefficient ψ, between $MgOH^+$, Mg^{2+}, and Cl^- at 25°C (Table 1). Only these act in the two systems Mg-Cl-OH-H_2O and Na-Mg-Cl-OH-H_2O and are not relevant for the well-described binary $Mg(OH)_2$-H_2O system; also there are no other complex Mg, Cl, and OH-containing systems for which experimental data are available, so adjustments were made. Based on the solubility data in the Mg-Cl-OH-H_2O system at 25°C (Pannach et al., 2017), systematic fit tests were performed. Both $\beta^{(0)}$ alone and with $\beta^{(1)}$, as well as with and without $\psi_{MgOH^+\text{-}Mg^{2+}\text{-}Cl^-}$ (and also ψ alone), were fitted. Furthermore, the parameters $C^{\phi}_{MgOH^+\text{-}Cl^-}$ and $\psi_{MgOH^+\text{-}OH^-\text{-}Cl^-}$ not included in the dataset were also tested. However, no results could be obtained that sufficiently described the analyzed total OH^- concentrations. When fitting the data at higher temperatures (available up to 120°C for the Mg-Cl-OH-H_2O system), the deviation was even greater than at 25°C.

4.2.2 Further complex Mg-OH solution species

Since the modeling of OH^- concentrations is not improved by Pitzer coefficients, it is assumed that, besides $MgOH^+$, further Mg-OH species that influence OH^- concentration must exist in the solution.

As known from other aqueous metal oxide or hydroxide salt systems, such as Be, Cu, Ni, and Zn (Feitknecht and Schindler, 1963; Mesmer and Baes, 1990; Plyasunova et al., 1997; 1998; Zhang and Muhammed, 2001), the existence of complex Mg-OH species containing more than one cation $Mg_x(OH)_y^{(2x-y)+}$ has been already discussed (D'Ans and Katz, 1941; Ved et al., 1976; Mesmer and Baes, 1990). Stability constants (Lewis, 1963; Einaga, 1977) alongside $MgOH^+$ (McGee and Hostetler, 1977; Palmer and Wesolowski, 1997) have also been proposed. Einaga (1977) derives the species $Mg_2(OH)_2{}^{2+}$ and $Mg_3(OH)_4{}^{2+}$ from emf measurements in nitrate solutions at 25°C with the stability constants log β = −22.0 and log β = −39.0, respectively. However, the determination of complex Mg-OH solution species lacks sufficient resolution to precisely determine the formulas, especially when more than one species coexists over a range of solution compositions. As Mg^{2+} is exclusively octahedrally coordinated by OH^- (partly together with OH_2) in these solids ($Mg(OH)_2$, Sorel phases 3-1-8, 5-1-8, and 9-1-4 (De Wolf and Walter-Lévy, 1953; Sugimoto et al., 2007; Dinnebier et al., 2010)),

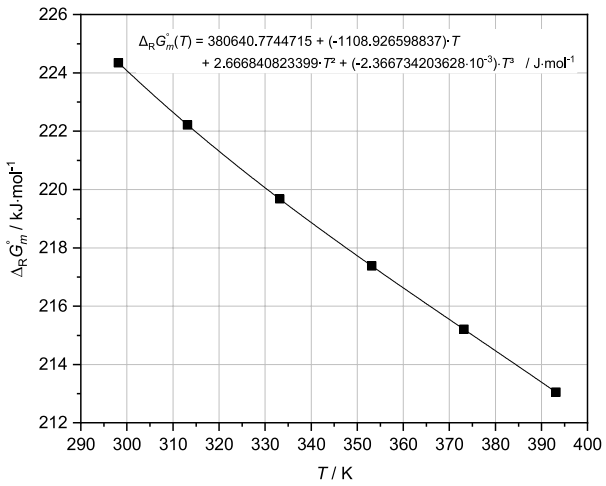

FIGURE 5
$\Delta_R G_m^\circ$ values for the solution species $Mg_3(OH)_4^{2+}$ derived from adjustments to the solubility data available at different temperatures in the Mg-Cl-OH-H_2O system, with the temperature function (black curve) fitted to these values (see also Table 3).

multiple OH^- coordinated Mg ions, in addition to $MgOH^+$ = $[Mg(H_2O)_5OH]^+$, could be expected to exist in appropriate equilibrium solutions.

Therefore, additional species were postulated based on the following considerations. In contrast to the solid structures with up to six OH^- ions in the octahedral coordination sphere of Mg^{2+}, the OH^- concentration in the equilibrium solution is relatively very low compared to the Mg^{2+} (and Cl^-) concentration. Thus, besides $MgOH^+$, additional solution-Mg^{2+} should be only slightly more highly coordinated with OH^-. Hence, species with a systematically increasing ratio of OH^- to Mg^{2+} up to a maximum of two were taken into account—$Mg_3(OH)_4^{2+}$ (ratio = 1.33), $Mg_2(OH)_3^+$ (ratio = 1.5), and $Mg(OH)_2^{\pm 0}$ (ratio = 2)—and were tested for their effect. Estimated $\Delta_R G_m^\circ$ values were used, in orientation to the value of $MgOH^+$ and the stability constant for $Mg_3(OH)_4^{2+}$ given by Einaga (1977), to first see the general effects. $Mg_2(OH)_2^{2+}$ was not taken into account because the Mg:OH ratio is the same as in $MgOH^+$ (tests have shown that the different charge does not have an effect). Calculations with the current THEREDA model show that $MgOH^+$ determines the total OH^- concentration, so the fraction of free OH^- is negligible. Fitting studies with the additional three postulated species were performed both singularly and in combinations.

Finally, the fitting tests to the 25°C isotherm in the Mg-Cl-OH-H_2O system (Pannach et al., 2017) showed that the total OH^- concentrations can be reproduced when including additional Mg-OH species. It was found that the species $Mg_3(OH)_4^{2+}$ alone was sufficient. The other species, alone or in combination, worsened the agreement with experimental results. Therefore, the final fits to all isotherms in the system Mg-Cl-OH-H_2O were performed with $Mg_3(OH)_4^{2+}$ additionally in the THEREDA dataset, turning off all ion interactions for $MgOH^+$ (see Table 1). $\Delta_R G_{m,Mg_3(OH)_4^{2+}}^\circ$ (according to the formation reaction: $3Mg^{2+} + 4H_2O \leftrightarrow Mg_3(OH)_4^{2+} + 4H^+$) was adjusted so that the isothermal branch of $Mg(OH)_2$(s) up to the invariant point with the 3-1-8 phase will be reproduced in agreement with the experimental data. With increasing $MgCl_2$ concentration, the total OH^- concentration in the presence of the 3-1-8 phase is calculated to be increasingly too high until $MgCl_2$ saturation is reached. This overestimation was subsequently adjusted with the final Pitzer coefficients (Section 4.2.3). The resulting values of $\Delta_R G_{m,Mg_3(OH)_4^{2+}}^\circ$ for each temperature are shown in Figure 5, together with the fitted temperature function (Table 3).

4.2.3 Final Pitzer coefficients

To remove the over-calculated total OH^- concentrations following the IP of $Mg(OH)_2$(s) and the 3-1-8 phase caused by the implementation of $Mg_3(OH)_4^{2+}$, ion interactions for that species were introduced. Fitting tests were carried out with binary as well as mixing Pitzer coefficients. Finally, the mixing parameter $\psi_{Mg\text{-}Mg_3(OH)_4\text{-}Cl}$ was

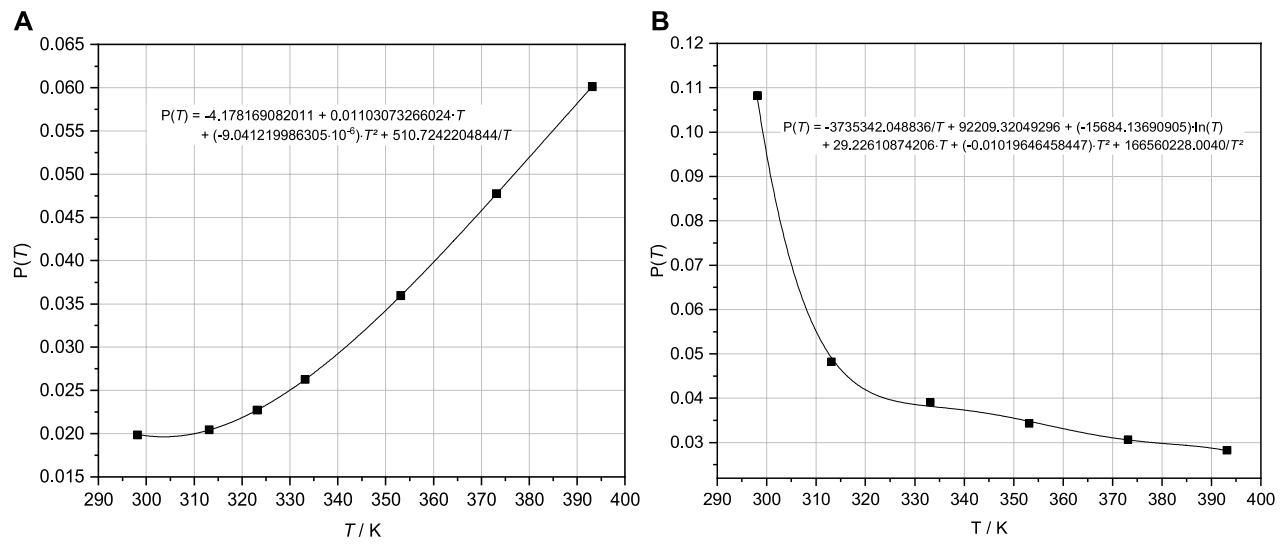

FIGURE 6
Pitzer coefficients $\psi_{Mg\text{-}MgOH\text{-}Cl}$ **(A)** and $\psi_{Mg\text{-}Mg3(OH)4\text{-}Cl}$ **(B)** resulting from fits to the isotherms in the Mg-Cl-OH-H_2O system (Pannach et al., 2017) and fitted temperature functions (Eq. 8).

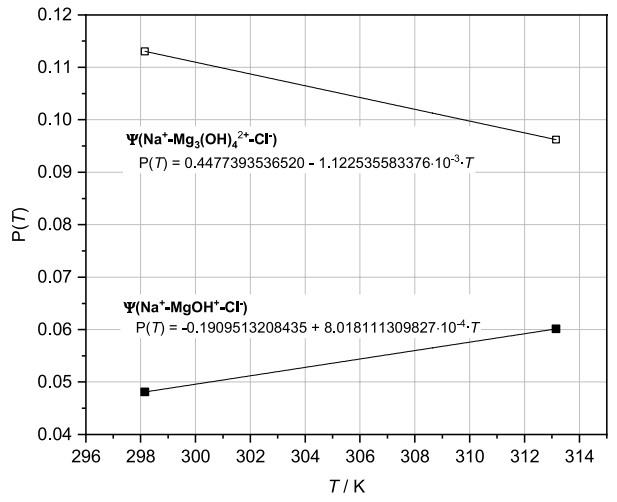

FIGURE 7
Pitzer coefficients $\psi_{\text{Na-MgOH-Cl}}$ and $\psi_{\text{Na-Mg3(OH)4-Cl}}$ resulting from adjustments to both the isotherms in the Na-Mg-Cl-OH-H_2O system (Part I = Pannach et al., 2023) and fitted temperature functions (Eq. 7).

adjusted together with $\psi_{\text{Mg-MgOH-Cl}}$. The binary coefficients $\beta^{(0)}$ and $\beta^{(1)}$ between $MgOH^+$ and Cl^- previously included beside the mixing $\psi_{\text{Mg-MgOH-Cl}}$ proved unnecessary; they were removed from the dataset. The parameterization was again performed separately on each isotherm. The obtained values for $\psi_{\text{Mg-Mg}_3\text{(OH)}_4\text{-Cl}}$ and $\psi_{\text{Mg-MgOH-Cl}}$ are shown in Figures 6A, B. The THEREDA conformal temperature function (Eq. 8) was fitted to the systematic variation of the parameters with T obtained from the isothermal fits (Figure 6).

$$P = \frac{a}{T} + b + c \cdot \ln(T) + d \cdot T + e \cdot T^2 + \frac{f}{T^2}. \quad (8)$$

Due to the polynomial type of the function (Eq. 8), the course for $\psi_{\text{Mg-Mg3(OH)4-Cl}}$ with the strong decrease from the 25°C value to the only slightly decreasing values up to 120°C can only be adjusted with turning points (Figure 6B). However, this does not show any noticeable effects on the model results within the experimental data trend and reproduction (Section 4.2).

For the modeling of the two solubility isotherms in the system Na-Mg-Cl-OH-H_2O at 25°C and 40°C, the implementation and adjustment of the mixing parameters $\psi_{\text{Na-MgOH-Cl}}$ and $\psi_{\text{Na-Mg}_3\text{(OH)}_4\text{-Cl}}$ were still necessary. The fitted values with linear progression over the two temperatures are shown in Figure 7.

All Pitzer coefficients with their temperature functions are listed in Table 4.

5 Calculation results with the extended THEREDA model

5.1 Modeling of H^+ equilibrium concentrations

With the addition of the $\Delta_R G_m^\circ$ temperature functions for the Sorel phases 3-1-8, 2-1-4, and 9-1-4 and for the metastable 5-1-8 phase at 25°C to the THEREDA dataset, the H^+ equilibrium concentrations can be calculated in good agreement with the experimental data. Figure 8 shows the comparison for the Mg-Cl-OH-H_2O system and Figure 9 for the Na-Mg-Cl-OH-H_2O system at NaCl saturation. Calculation results between and just outside the temperatures of the experimental data are still included, showing that the model reliably calculates the occurring solids depending on $MgCl_2$ solution concentration and the pH_m = -lg m (H^+), evolving in their presence over the entire and somewhat extended temperature field.

5.2 Modeling of OH^- equilibrium concentrations

The implementation of a second Mg-OH solution species, $Mg_3(OH)_4^{2+}$, was the key to the accurate calculation of the OH^- solution concentrations in equilibrium with $Mg(OH)_2$(s) or the Sorel phases. Still requiring mixing Pitzer coefficients, $\psi_{\text{Mg-Mg3(OH)4-Cl}}$ and $\psi_{\text{Na-Mg3(OH)4-Cl}}$, were introduced and fitted together with $\psi_{\text{Mg-MgOH-Cl}}$ or $\psi_{\text{Na-MgOH-Cl}}$ for final adjustment to the solubility isotherms in the Mg-Cl-OH-H_2O (Nakayama, 1959; Nakayama, 1960; Pannach et al., 2017) and Na-Mg-Cl-OH-H_2O systems (Part I of this work—Pannach et al., 2023), respectively.

Finally, the solubilities can be calculated in agreement with all experimental data. As Figure 10A shows for the Mg-Cl-OH-H_2O system at 25°C, the total OH^- concentration is mainly a result of the $MgOH^+$ solution species over the entire concentration range but in addition from lesser proportions of $Mg_3(OH)_4^{2+}$ with the highest contribution at the $MgCl_2$ concentration of the IP $Mg(OH)_2$(s) and 3-1-8 phase. This now leads to a correct representation of the total OH^- concentration. With increasing temperature, $Mg_3(OH)_4^{2+}$ becomes increasingly predominant over $MgOH^+$, as shown in Figure 10B for the 60°C isotherms as an example in comparison to 25°C (Figure 10A). The contribution of free OH^- in the order of 10^{-9} molal at 60°C (10^{-5} molal at 25°C) is insignificant: its proportion is unaffected by the implementation of the second Mg-OH species since it is calculated together with H^+ from Kw (Eq. 9), which is already included in the model (Figure 11 shows Kw, H^+, and OH^- as a function of the $MgCl_2$ solution concentration according to the HMW and THEREDA model at 25°C). This also justifies the already-correct calculation of the H^+ solution concentrations in the presence of $Mg(OH)_2$(s) or the Sorel phases with the previous model; it also confirms that the earlier poor model description of the total OH^- solution concentrations is due to missing further Mg-OH speciation.

$$K_W^0 = \frac{[H^+] \cdot [OH^-] \cdot \gamma_\pm^2}{a_W} = \frac{K_W \cdot \gamma_\pm^2}{a_W}. \quad (9)$$

The calculation results for the Mg-Cl-OH-H_2O system compared to all reliable experimental datasets are shown in Figure 12. Within their experimental scatter range, the calculated $Mg(OH)_2$(s) isotherms overlie each other, with ranges extending toward higher $MgCl_2$ concentrations up to the positions of the IPs with the Sorel phases. The subsequent isotherms for the 3-1-8 phase (stable phase up to 80°C) or the 9-1-4 phase (from 100 °C) effectively describe the course of the experimental values. For the 9-1-4 phase, the IPs with brucite and the isotherms at 100°C and 120°C are

10.3389/fnuen.2023.1236544

TABLE 4 Temperature coefficients of Pitzer parameters for the title system Na-Mg-Cl-OH-H_2O and subsystem in THEREDA. The new data from this work are highlighted in bold.

$P(T) = a/T + b + c\cdot\ln(T) + d\cdot T + e\cdot T^2 + f/T^2$								
			a	b	c	d	e	f
H^+	Cl^-	Beta (0)	9901.2219784713	−285.6473091587	50.067215202357	−0.10902829201997	4.2832131817909E-5	−351026.15442901
		Beta (1)	189788.67075591	−4588.8079271153	776.48444741115	−1.3963936941488	4.6718218052799E-4	−8599260.9958506
		Cphi	0	0	0	0	0	0
Na^+	Cl^-	Beta (0)	9931.0954	−223.8321	37.468729	−0.063524	2.0008E-5	−508663.3
		Beta (1)	27034.783	−611.8806	102.2781	−0.171355	5.4624E-5	−1335514
		Cphi	−4635.055	107.86756	−18.11616	0.0311444	−9.9052E-6	221646.78
Mg^{2+}	Cl^-	Beta (0)	−9.5949075987732	0.52058075085694	0	−4.5632571158819E-4	0	0
		Beta (1)	1239.2880942931	−7.3631696542185	0	0.016394622815563	0	0
		Cphi	12.528229322268	−0.045346523422936	0	2.8564736424319E-5	0	0
Na^+	OH^-	beta (0)	−98.888405195742	0.74845113296049	0	−0.0010478515797703	0	0
		Beta (1)	−206.11199903783	1.2022295299777	0	−0.0012958058812917	0	0
		Cphi	17.300056299236	−0.091131605628721	0	1.1826675205965E-4	0	0
Na^+	H^+	Theta	−4.0542575885501	0.048135767274039	0	0	0	0
Na^+	Mg^{2+}	Theta	0	−0.063343456551807	0	4.4723332094534E-4	0	0
Mg^{2+}	H^+	Theta	0	0.51653862168501	0	−0.0031309680558061	5.8285013290036E-6	0
OH^-	Cl^-	Theta	−49.361345504841	0.11048570304889	0	0	0	0
psi								
Na^+	Cl^-	OH^-	0	−3.61342282638764	0.828412891695231	−0.00473162879186962	3.37394750135306E-6	0
Na^+	Mg^{2+}	Cl^-	0	−2.67633662036202	0.618873156654038	−0.00367854306693126	2.64366820374045E-6	0
Na^+	H^+	Cl^-	3.59304603523964	−0.0145621583979794	0	0	0	0
Mg^{2+}	H^+	Cl^-	−1357.291354862	61.244574321968	−11.309231470323	0.029270572012749	−1.1173505755006E-5	−33.683663900415
Na^+	**$MgOH^+$**	**Cl^-**	**0**	**−0.1909513208435**	**0**	**0.008018111309827**	**0**	**0**
Na^+	**$Mg_3(OH)_4^{2+}$**	**Cl^-**	**0**	**0.4477393536520**	**0**	**−0.001122535583376**	**0**	**0**
Mg^{2+}	**$MgOH^+$**	**Cl^-**	**510.7242204844**	**−4.178169082011**	**0**	**0.01103073266024**	**−9.041219986305E-6**	**0**
Mg^{2+}	**$Mg_3(OH)_4^{2+}$**	**Cl^-**	**−3735342.048836**	**92209.32049296**	**−15684.13690905**	**29.22610874206**	**−0.01019646458447**	**166560228.0040**

alpha (1) = 2 and alpha (2) = 0 for all binary ion interactions.

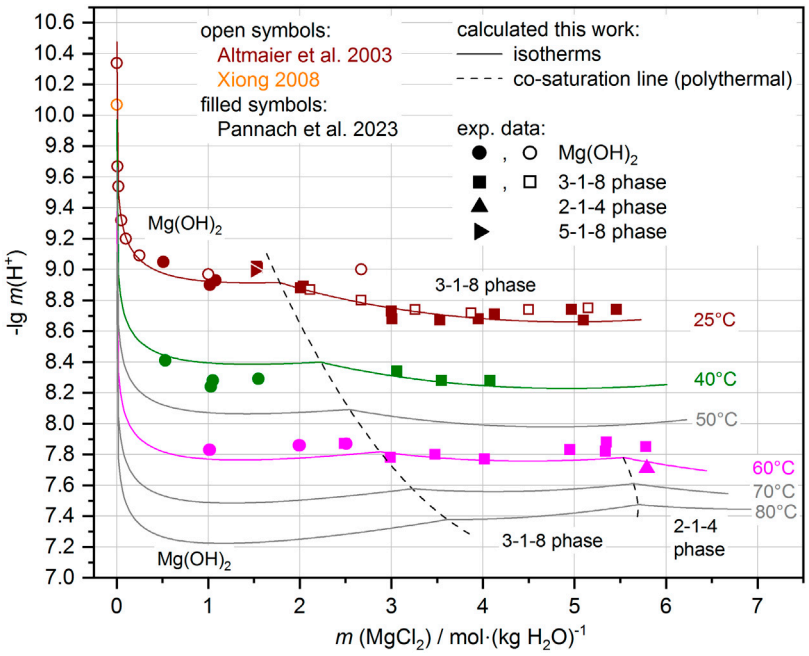

FIGURE 8
Comparison of experimental and calculated pH_m = -lg m (H^+) in the Mg-Cl-OH-H_2O system. Experimental data available at 25°C, 40°C, and 60°C (see also Pannach et al., 2023). Away from these temperatures, the model shows systematic trends (gray lines calculations at 50°C, 70°C, and 80°C, and the dashed co-saturation lines of the $Mg(OH)_2$(s) and 3-1-8 phase, and the 3-1-8 and 2-1-4 phases respectively) that follow the experimental data.

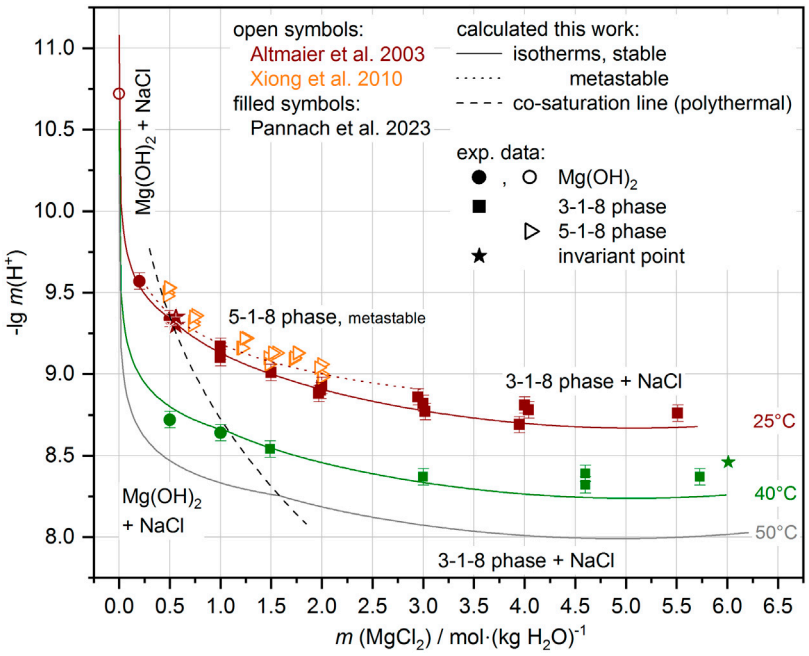

FIGURE 9
Comparison of experimental and calculated pH_m in almost NaCl-saturated $MgCl_2$ solutions (system Na-Mg-Cl-OH-H_2O). Experimental data available at 25°C and 40°C (see also Pannach et al., 2023). Away from these temperatures, the model shows systematic trends (gray lines for 50 C and dashed co-saturation line of $Mg(OH)_2$(s) and 3-1-8 phase) that follow the experimental data.

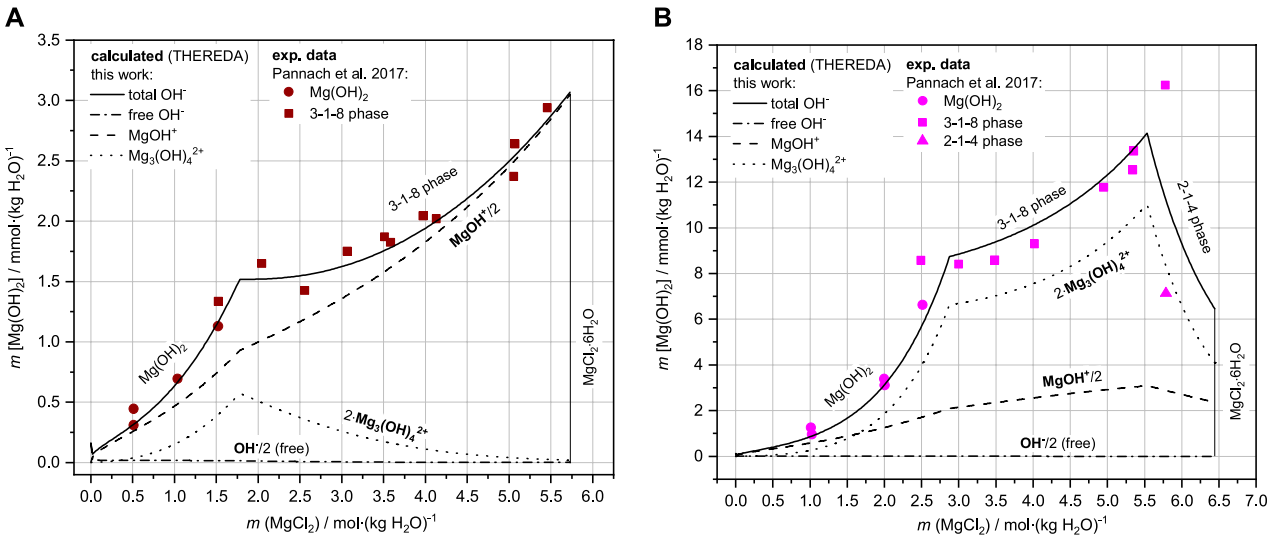

FIGURE 10
Comparison of experimental and calculated (with OH-species distribution) solubility data of $Mg(OH)_2$(s) and 3-1-8 phase in the Mg-Cl-OH-H_2O system at 25°C **(A)** and 60°C **(B)**.

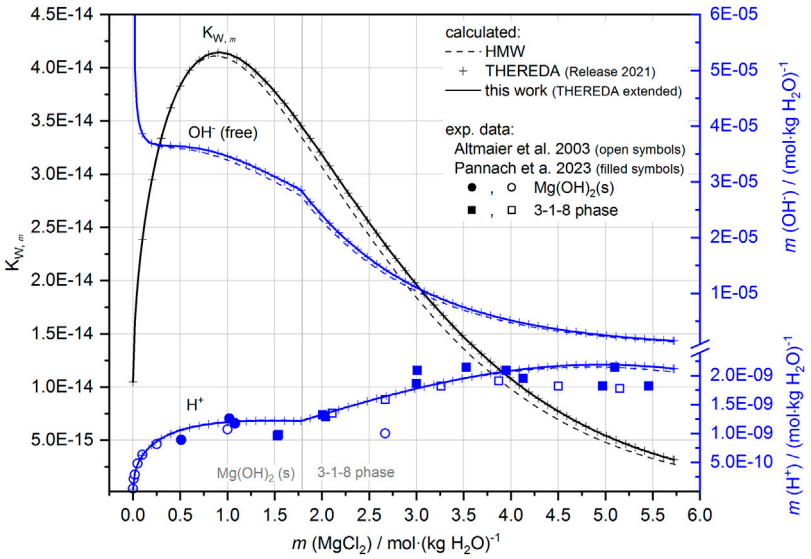

FIGURE 11
$K_{W,m}$, H^+ (comparison with experimental data, cf. Figure 8) and OH^- as a function of the $MgCl_2$ solution concentration (system Mg-Cl-OH-H_2O) according to the HMW and THEREDA models at 25°C.

calculated nearly exactly in line with the experimental data. The calculated isotherm for the metastable 3-1-8 phase at 100°C is slightly below the experimental values but on trend; it is above the 9-1-4 phase 100°C isotherm.

The 2-1-4 phase, occurring above 60°C at high $MgCl_2$ concentrations with its strongly decreasing solubility behavior up to the $MgCl_2$ saturation concentrations, is calculated in conformity with the experimental (more scattering) values. The calculated isotherm, especially at 100°C, is shifted to slightly higher values compared with the trend of the experimental dataset. When using the isothermally determined $\Delta_R G_m^\circ$ value of the 2-1-4 phase (see Section 4.1.2), a somewhat better agreement with the experimental data would result. However, since the temperature function does not reproduce the individually determined $\Delta_R G_m^\circ$ value to 100% ($\Delta_R G_{m,2\text{-}1\text{-}4,100°C}^\circ$ = 205.6 kJ mol^{-1} is calculated by the temperature function with 205.8 kJ mol^{-1}), the model result via temperature function deviates somewhat. Furthermore, with increasing temperature and $MgCl_2$ concentration, the possible existence of further Mg-OH solution species must be assumed, also affecting solubility. However, without experimental evidence and data, the

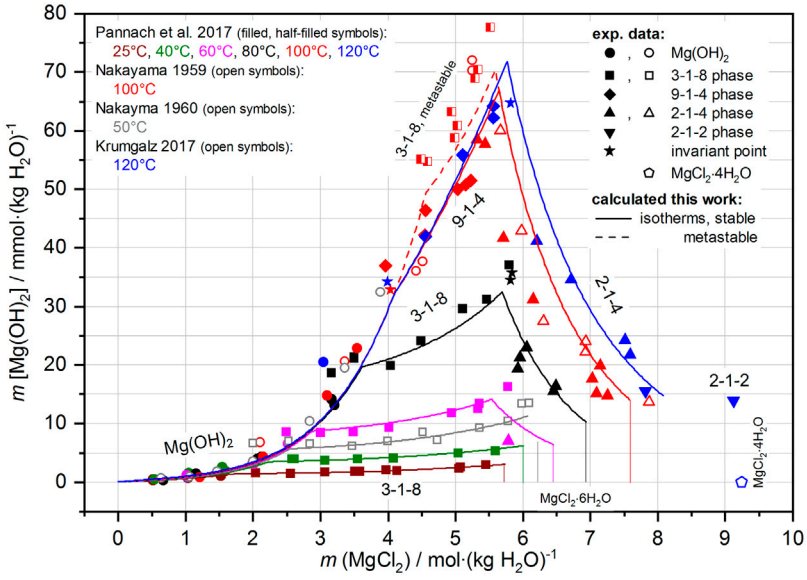

FIGURE 12
Solubility data of the Mg-Cl-OH-H_2O system from 25°C to 120°C; comparison of the experimental data with the calculated isotherms.

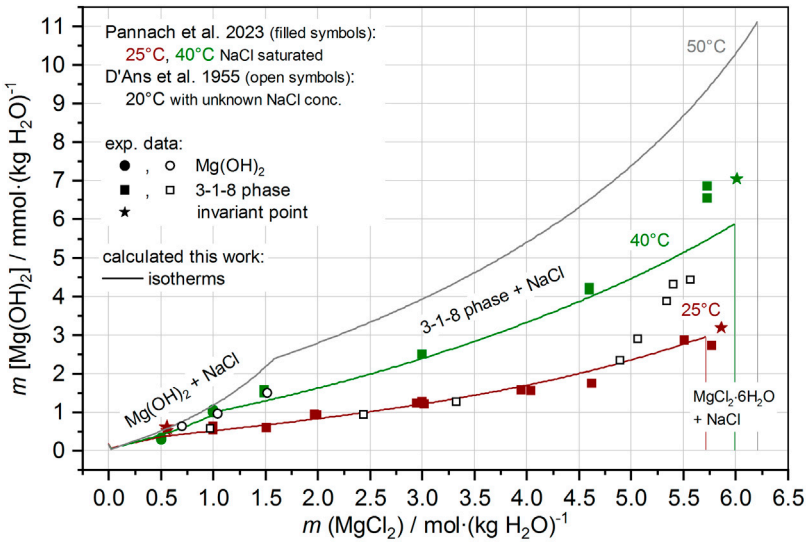

FIGURE 13
Solubility data of the Na-Mg-Cl-OH-H_2O system with NaCl saturation at 20°C–50°C; comparison of the experimental data with the calculated isotherms.

model cannot be further modified. With the present model (THEREDA extended), the solubility behavior of $Mg(OH)_2$(s) and the Sorel phases can be described quite well up to 120°C. This is also true in the presence of NaCl saturation in the Na-Mg-Cl-OH-H_2O system, as shown by the comparison of the experimental datasets at 25°C and 40°C and the calculated isotherms in Figure 13. The additional calculated isotherms for 50°C indicate a reasonable trend with the IP of the $Mg(OH)_2$(s) and 3-1-8 phase in an approximately 1.6 molal solution of $MgCl_2$ (at 25°C and 40°C in 0.5 and ca. 1 molal solution, respectively).

The 2-1-2 phase, with only two solubility data points at 120°C in the Mg-Cl-OH-H_2O system (Figure 12), was not included in the model.

6 Summary

With this work, the Pitzer model dataset of THEREDA was extended and adjusted for the calculation of the solubility equilibria of the Sorel phases and of $Mg(OH)_2$(s) in salt solutions of the system Na-Mg-Cl-OH-H_2O.

Previously, calculations were possible only with strong deviations from the now available experimental OH^- solution concentrations of the 25°C isotherms of $Mg(OH)_2$(s) as well as the Sorel phase 3-1-8, although the H^+ concentrations could be calculated in agreement. The Pitzer dataset, corresponding to the HMW model and implemented in THEREDA, was valid only for 25°C; due to the lack of experimental data, no sufficient adjustments were possible.

With the data now available for the Mg-Cl-OH-H_2O system up to 120°C and in NaCl-saturated solutions (Na-Mg-Cl-OH-H_2O system) at 25°C and 40°C within Part I of this work, a new adjustment of the model and polytherm was possible. In addition to the implementation of the solubility constants for the Sorel phases as temperature functions of molal standard Gibbs energies of formation, a model extension for the OH^- solution speciation (the implementation of $Mg_3(OH)_4^{2+}$ in addition to $MgOH^+$ and OH^-) was necessary to reproduce the experimentally determined OH^- solution concentrations. Thus, the solubility equilibria of the Sorel phases and $Mg(OH)_2$(s) can now be calculated in agreement with the experimental data.

THEREDA now provides a reliable database for the long-term safety assessment of geotechnical barriers made of Sorel cement/concrete for a repository in host rock salt. It also allows the calculation of the evolving pH_m values (caused by the pH buffer material MgO which reacts to Sorel phases or $Mg(OH)_2$ in the presence of salt solutions), which is particularly important for predictions regarding the retention capacity of radionuclides in the near field of a repository.

Data availability statement

The raw data supporting the conclusion of this article will be made available by the authors, without undue reservation.

Author contributions

DF: procedure for the extension of the Pitzer model dataset and writer of the paper. MP: calculation tests, adjustments, preparation of figures and tables, and co-writer. WV: Pitzer model expert, discussions and contributions to dataset development, and co-writer. All authors contributed to the article and approved the submitted version.

Funding

This research was supported by the Open Access Funding by the Publication Fund of the TU Bergakademie Freiberg.

Conflict of interest

The authors declare that the research was conducted in the absence of any commercial or financial relationships that could be construed as a potential conflict of interest.

Publisher's note

References

Altmaier, M., Metz, V., Neck, V., Müller, R., and Fanghänel, T. (2003). Solid-liquid equilibria of $Mg(OH)_2$(cr) and $Mg_2(OH)_3Cl{\cdot}4H_2O$(cr) in the system Mg-Na-H-OH-Cl-H_2O at 25°C. *Geochim. Cosmochim. Acta* 67 (19), 3595–3601. doi:10.1016/s0016-7037(03)00165-0

D'Ans, J., Busse, W., and Freund, H. E. (1955). Basic magnesium chloride. *Kali Steinsalz* 8, 3–7.

D'Ans, J., and Katz, W. (1941). The solubility of magnesium hydroxide, the pH value and buffering in the system H2O-MgCl2-Mg(OH)2. *Kali Steinsalz* 35, 37–41.

De Wolf, P. M., and Walter-Lévy, L. (1953). The crystal structure of $Mg_2(OH)_3$(Cl, Br)·$4H_2O$. *Acta Cryst.* 6, 40–44. doi:10.1107/s0365110x53000089

Dinnebier, R. E., Freyer, D., Bette, S., and Oestreich, M. (2010). $9Mg(OH)_2{\cdot}MgCl_2{\cdot}4H_2O$, a high temperature phase of the magnesia binder system. *Inorg. Chem.* 49, 9770–9776. doi:10.1021/ic1004566

Einaga, H. (1977). Hydrolysis of magnesium(II) in 1.0 mol dm^{-3} aqueous (Na,H)NO_2 solution. *J. Chem. Soc. Dalton Trans. Inorg. Chem.* 9, 912–914. doi:10.1039/DT9770000912

Eriksson, G., and Hack, K. (1990). ChemSage - a computer program for the calculation of complex chemical equilibria. *Metall. Trans.* B21 (6), 1013–1023. doi:10.1007/bf02670272

Eriksson, G., Hack, K., and Petersen, S. (1997). "ChemApp - a programable thermodynamic calculation interface," in Werstoffwoche '96, Symposium 8: Simulation, Modellierung, Informationssysteme (Deutschland: DGM Informationsgesellschaft mbH).

Feitknecht, W., and Schindler, P. (1963). Solubility constants of metal oxides, metal hydroxides, and metal hydroxide salts in aqueous solution. *Pure Appl. Chem.* 6, 125–206. doi:10.1351/pac196306020125

Harvie, C. E., Møller, N., and Weare, J. H. (1984). The prediction of mineral solubilities in natural waters: na-K-Mg-Ca-H-Cl-SO_4-OH-HCO_3-CO_3-CO_2-H_2O system to high ionic strengths at 25°C. *Geochim. Cosmochim. Acta* 48, 723–751. doi:10.1016/0016-7037(84)90098-x

Krumgalz, B. S. (2017). Temperature dependence of mineral solubility in water. Part I. Alkaline and alkaline earth chlorides. *J. Phys. Chem. Ref. Data* 46 (4). AIP Publishing. doi:10.1063/1.5006028

Lambert, I., and Clever, H. L. (1992). "Alkaline earth hydroxides in water and aqueous solutions," in *IUPAC solubility data series* (Oxford, UK: Pergamon Press), 52.

Lewis, D., Lund, A., Vänngård, T., Håkansson, R., and Munch-Petersen, J. (1963). Studies on the hydrolysis of metal ions. 45. The hydrolysis of magnesium in chloride self-medium. *Acta Chem. Scand.* 17 (7), 1891–1901. doi:10.3891/acta.chem.scand.17-1891

McGee, K. A., and Hostetler, P. B. (1977). Activity-product constants of brucite from 10° to 90°C. *J. Res. U.S. Geol. Surv.* 5 (2), 227–233.

Mesmer, R. E., and Baes, C. F. (1990). Review of hydrolysis behavior of ions in aqueous solutions. *Mat. Res. Soc. Symp. Proc.* 180, 85–96. doi:10.1557/proc-180-85

Nakayama, M. (1959). A new basic triple salt containing magnesium hydroxide Part II. The quaternary system KCl-$MgCl_2$-$Mg(OH)_2$-H_2O at 100°. *Bull. Agr. Chem. Soc. Jpn.* 23(1), 46–48. doi:10.1080/03758397.1959.10857524

Nakayama, M. (1960). A new basic triple salt containing magnesium hydroxide Part IV. The quinary system KCl-K_2SO_4-$MgCl_2$-$MgSO_4$-$Mg(OH)_2$-H_2O at 50°. *Bull. Agr. Chem. Soc. Jpn.* 24(4), 362–371. doi:10.1080/03758397.1960.10857688

Palmer, D. A., and Wesolowski, D. J. (1997). Potentiometric measurements of the first hydrolysis quotient of magnesium(II) to 250°C and 5 molal ionic strength (NaCl). *J. Solut. Chem.* 26 (2), 217–232. doi:10.1007/bf02767923

Pannach, M., Bette, S., and Freyer, D. (2017). Solubility equilibria in the system $Mg(OH)_2$-$MgCl_2$-H_2O from 298 to 393 K. *J. Chem. Eng. Data* 62 (4), 1384–1396. doi:10.1021/acs.jced.6b00928

Pannach, M., Paschke, I., Metz, V., Altmaier, M., Voigt, W., and Freyer, D. (2023). Solid-liquid equilibria of Sorel phases and $Mg(OH)_2$ in the system Na-Mg-Cl-OH-H_2O. Part I: experimental determination of OH^- and H^+ equilibrium concentrations and solubility constants at 25°C, 40°C and 60°C. *Front. Nuc. Eng.* 2. doi:10.3389/fnuen.2023.1188789

Pitzer, K. S. (1991). *Activity coefficients in electrolyte solutions*. 2. Edition. Boca Raton: CRC Press.

Plyasunova, N. V., Wang, M., Zhang, Y., and Muhammed, M. (1997). Critical evaluation of thermodynamics of complex formation of metal ions in aqueous solutions II. Hydrolysis and hydroxo-complexes of Cu^{2+} at 298.15 K. *Hydrometallurgy* 45 (1-2), 37–51. doi:10.1016/s0304-386x(96)00073-4

Plyasunova, N. V., Zhang, Y., and Muhammed, M. (1998). Critical evaluation of thermodynamics of complex formation of metal ions in aqueous solutions. IV. Hydrolysis and hydroxo-complexes of Ni^{2+} at 298.15 K. *Hydrometallurgy* 48 (1), 43–63. doi:10.1016/s0304-386x(97)00070-4

Robinson, W. O., and Waggaman, W. H. (1909). Basic magnesium chlorides. *J. Phys. Chem.* 13, 673–678. doi:10.1021/j150108a002

Sugimoto, K., Dinnebier, R. E., and Schlecht, T. (2007). Structure determination of $Mg_3(OH)_5Cl{\cdot}4H_2O$ (F5 phase) from laboratory powder diffraction data and its impact on the analysis of problematic magnesia floors. Acta Cryst. *B* 63, 805–811. doi:10.1107/S0108768107046654

THEREDA (2021). *Thermodynamic reference database*. Release (2021). Available at: www.thereda.de.

Travers, A. (1929). The solubility of magnesium hydroxide at elevated temperatures. *C. R. Acad. Sci.* 188, 499–501.

Ved, E. I., Zharov, E. F., and Hoang, V. P. (1976). Mechanism of magnesium oxychloride formation during the hardening of magnesia cements. *Zh. Prikl. Khim.* 49, 2154–2158.

Voigt, W., Brendler, V., Marsh, K., Rarey, R., Wanner, H., Gaune-Escard, M., et al. (2007). Quality assurance in thermodynamic databases for performance assessment studies in waste disposal. *Pure Appl. Chem.* 79 (5), 883–894. doi:10.1351/pac200779050883

Xiong, Y., Deng, H., Nemer, M., and Johnsen, S. (2010). Experimental determination of the solubility constant for magnesium chloride hydroxide hydrate ($Mg_3Cl(OH)_5{\cdot}4H_2O$, phase 5) at room temperature, and its importance to nuclear waste isolation in geological repositories in salt formations. *Geochim. Cosmochim. Acta* 74, 4605–4611. doi:10.1016/j.gca.2010.05.029

Xiong, Y. (2008). Thermodynamic properties of brucite determined by solubility studies and their significance to nuclear waste isolation. *Aquat. Geochem.* 14 (3), 223–238. doi:10.1007/s10498-008-9034-3

Zhang, Y., and Muhammed, M. (2001). Critical evaluation of thermodynamics of complex formation of metal ions in aqueous solutions VI. Hydrolysis and hydroxo-complexes of Zn^{2+} at 298.15 K. *Hydrometallurgy* 60 (3), 215–236. doi:10.1016/s0304-386x(01)00148-7